Congreso Internacional Conjunto Cancún 2004 LAS/ANS-SNM-SMSR/International Joint Meeting Cancun 2004 LAS/ANS-SNM-SMSR
XV Congreso Anual de la SNM y XXII Reunión Anual de la SMSR/XV SNM Annual Meeting and XXII SMSR Annual Meeting
Cancún, Q.R., México, 11-14 de Julio, 2004/Cancún, Q.R., Mexico, July 11-14, 2004

Effective Dose Conversion Coefficients for X-ray Radiographs of the Chest and the Abdomen

F. R. A. Lima
Centro Regional de Ciências Nucleares, CRCN/CNEN
Rua Cônego Barata, 999, Tamarineira, Recife, PE, Brazil
and
Faculdade Boa Viagem
Boa Viagem, Recife, Brazil
falima@cnen.gov.br

R. Kramer, J. W. Vieira and H. J. Khoury
Departamento de Energia Nuclear, DEN/UFPE
Av. Prof. Luis Freire, 1000, Cidade Universitária, Recife, PE, Brazil
kramer@uol.com.br; jwvieira@br.inter.net; khoury@ufpe.br

Abstract

The recently developed MAX (*M*ale *A*dult vo*X*el) and the FAXht (*F*emale *A*dult vo*X*el) head and trunk phantoms have been used to calculate organ and tissue equivalent dose conversion coefficients for X-ray radiographs of the chest and the abdomen as a function of source and field parameters, like voltage, filtration, field size, focus-to-skin distance, etc. Based on the equivalent doses to twenty three organs and tissues at risk, the effective dose has been determined and compared with corresponding data for others phantoms. The influence of different radiation transport codes, different tissue compositions and different human anatomies have been investigated separately.

1. INTRODUCTION

Conversion coefficients (CCs) between absorbed dose or equivalent dose to organs at risk and measurable quantities commonly used in X-ray diagnosis have been calculated since 1976 mostly for mathematical MIRD-type phantoms [1-8]. The reported doses have generally been normalized to incident air kerma free-in-air at the surface of the patient (INAK), to entrance surface air kerma at the surface of the patient including backscatter (ESAK), or to the dose-area product (DAP). As tomographic or voxel phantoms have been developed only during recent years, few publications exist until now which used this new type of phantom for absorbed or equivalent dose calculations in X-ray diagnosis [9-10].

The recently developed MAX (*M*ale Adult *voXel*) [11] and FAXht (*F*emale *A*dult *voXel*) head and trunk phantoms [12] connected to the EGS4 Monte Carlo code [13] were used for an examination of the chest and the abdomen to calculate CCs between effective dose [14] and

ESAK at the center of the X-ray beam where it enters the phantom's body. The results will be compared with corresponding data calculated for this study with the mathematical ADAM and EVA phantoms, and data published for the NRPB MIRD-type phantom [3, 6 and 8].

2. MATERIALS AND METHODS

2.1 Exposure Models

2.1.1. The mathematical ADAM/EVA-GSF exposure model

The mathematical ADAM and EVA phantoms were introduced by Kramer et al [15] as gender-specific derivatives of the hermaphrodite MIRD phantom [16]. The form of the bodies and its organs are described by mathematical expressions representing planes, circular and elliptical cylinders, spheres, cones, tori, etc., and combinations and intersections thereof. Organ masses, body weights and body heights correspond to the anatomical data for adult males and females recommended in the first ICRP Reference Man Report, ICRP Publication No. 23 [17]. Figure 1 shows frontal views of the two phantoms.

The GSF Monte Carlo code uses a non-analogue method, which applies the same photon transport physics as the ALGAM code [20], the so-called fractional photon technique, in order to increase the number of photon scattering events in deeply penetrated areas of the phantoms body, thereby reducing the coefficient of variance. Rayleigh scattering and secondary electrons are not considered by this code. The photon cross-section data were taken from Roussin et al [21].

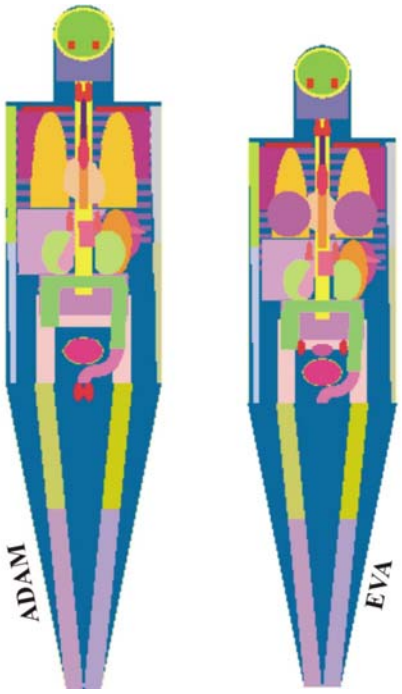

Figure 1. The mathematical ADAM and EVA phantoms

2.1.2 The voxel-based MAX/FAXht-EGS4 exposure model

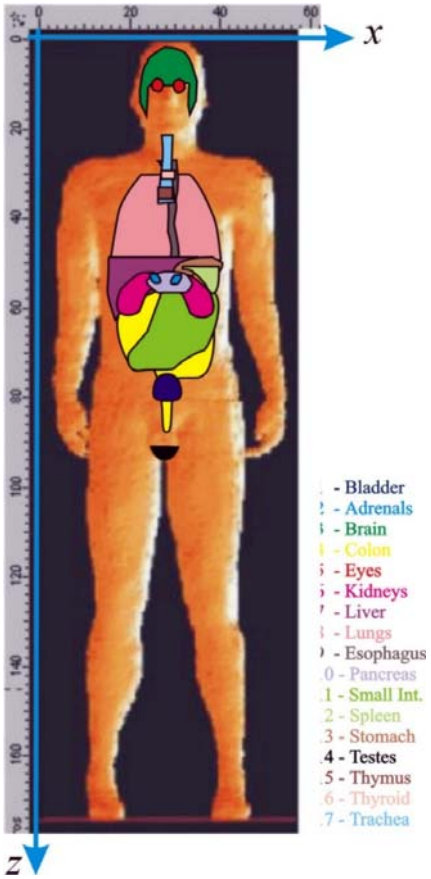

Figure 2a. The MAX phantom

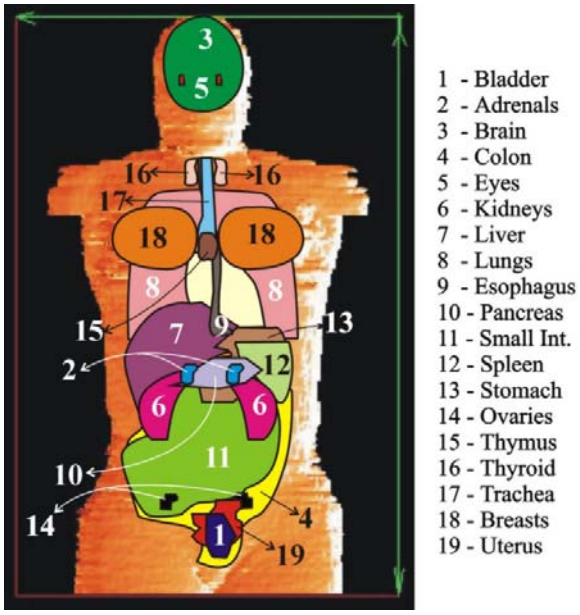

Figure 2b. The FAXht phantom

Figures 2a and 2b show frontal views of the MAX and the FAXht phantoms, respectively.

The MAX (*M*ale *A*dult *voXel*) phantom [11] and the FAXht (*F*emale *A*dult *voXel*) head and trunk phantom [12] are the first human voxel phantoms which correspond to the anatomical data recommended by the second ICRP Reference Man Report, Publication No. 89 [22], for most organs and tissues at risk. The two phantoms have been constructed based on CT images of patients. The MAX and the FAXht phantoms are connected to the EGS4 Monte Carlo code [13], which simulates coupled electron-photon transport through arbitrary media. The default version of EGS4 applies an analogue Monte Carlo method, which was used for the calculations of this investigation. Rayleigh scattering has normally been taken into account in the calculations. Although possible, secondary electrons have not been considered in the present calculations, because of the range of diagnostic photon energies and the quantities to be determined, namely equivalent dose to organs and tissues of the human body averaged over the volume of interest. The photon cross-sections were taken from Storm and Israel [23] and from Hubbell and Overbo [24].

Radiological examinations

From the data calculated for a variety of commonly performed radiographic examinations, this paper will present effective doses for examinations of the chest and the abdomen. The exposure conditions including the X-ray spectra [28] were the same used in the Monte Carlo calculations of the NRPB [3, 6, and 8] for a MIRD-type hermaphrodite phantom.

The chest examinations for the male phantoms were done for posterior-anterior (PA) projection with a focus-to-detector distance of 185cm, and a field size in the detector plane of 35cm x 44cm, while the abdominal examinations were simulated for anterior-posterior (AP) projection with a focus-to-detector distance of 85cm, and a filed size in the detector plane of 35cm x 47cm. The authors of the NRPB studies justify the use of field sizes larger than commonly used X-ray films with the argument, that thereby it was ensured that certain anatomical landmarks would appear inside the X-ray field according to the guidelines of X-ray practitioners, which indicates that inter-organ distances in the MIRD-type phantoms are sometimes too large.

For the female phantoms EVA and FAXht field sizes and the position of the center of the X-ray field were reduced by 7.4%, which corresponds to the difference found between the body heights of the male and the female reference persons [22].

All spectra used in the calculations represented an X-ray tube with constant potential generator, tungsten target, 17^0 anode angle, and 2.5mm Al total filtration. The coefficients of variance for the calculated effective doses were generally less than 2.5%.

Exposure conditions

The replacement of the ADAM/EVA-GSF exposure model by the MAX/FAXht-EGS4 exposure model implies changes with respect to Monte Carlo codes, tissue compositions, and phantom anatomies. The intention of this investigation is to study the dosimetric effect of each of these

parameters separately. Therefore the following five different exposure conditions a) – e) have been investigated:

Monte Carlo codes

ADEV/GSF: The mathematical ADAM and EVA phantoms connected to the GSF Monte Carlo code with tissue compositions used in Kramer et al [15] and Zankl et al [19];

ADEV: The mathematical ADAM and EVA phantoms connected to the EGS4 Monte Carlo code with the tissue compositions used for a);

ICRU44 tissue compositions

ADEV44: The mathematical ADAM and EVA phantoms connected to the EGS4 Monte Carlo code with tissue compositions taken from ICRU 44 [29], with a homogeneous mixture in all skeletal voxels based on ICRP70 [30], and a homogeneous mixture for adipose and muscle in all unspecified regions of the body.

Table I. Tissue compositions

ATOM	SOFT	SOFT	SKIN	SKIN	LUNGS	LUNGS	SKEL.	SKEL.	ADIMUS
	ADEV44	ADEV	ADEV44	ADEV	ADEV44	ADEV	ADEV44	ADEV	ADEV44
	[%]	[%]	[%]	[%]	[%]	[%]	[%]	[%]	[%]
H	10,5	10	10	10,2	10,3	10	7,2	7	10,6
C	12,5	23	20,4	26,9	10,5	10	31,3	23	30,8
N	2,6	2,3	4,2	4,3	3,1	2,8	3,2	3,9	2,4
O	73,5	63	64,5	58	74,9	76	41,1	49	55,4
Na	0,2	0,13	0,2	0,01	0,2	0,2	0,1	0,32	0,1
Mg		0,015		0,005		0,007	0,1	0,11	
P	0,2	0,24	0,1	0,3	0,2	0,08	5,3	6,9	0,128
S	0,18	0,22	0,2	0,15	0,3	0,23	0,25	0,17	0,227
Cl	0,22	0,14	0,3	0,25	0,3	0,27	0,1	0,14	0,1
K	0,21	0,21	0,1	0,1	0,2	0,2	0,05	0,15	0,245
Ca	0,01			0,14		0,007	11,3	9,9	
Fe	0,01	0,006		0,002		0,04		0,008	
$\rho[gcm^{-3}]$	1,05	0,98	1,09	1,105	0,26	0,296	1.469	(1.486)	1,012

SOFT = soft tissue; SKEL. = skeleton; ADIMUS: Homogeneous mixture of 36.2% Adipose + 63.8% Muscle.

Table I shows the tissue compositions for the ADEV phantoms, which represent the elemental mass fractions and densities taken from Kramer et al [15], while ADEV44 represent the new tissue compositions taken from ICRU Report No.44 [18]. The density of the ADEV skeletal mixture was later corrected to 1.4 $g.cm^{-3}$ [25]. ADIMUS represents a homogeneous mixture of 36.2% adipose and 63.8% muscle, which is the percentage distribution for the two tissues found in the MAX phantom. As the FAXht phantom is still uncompleted with respect to the total masses of adipose and muscle, a corresponding female percentage will be available only after the addition of legs and arms to the FAXht phantom.

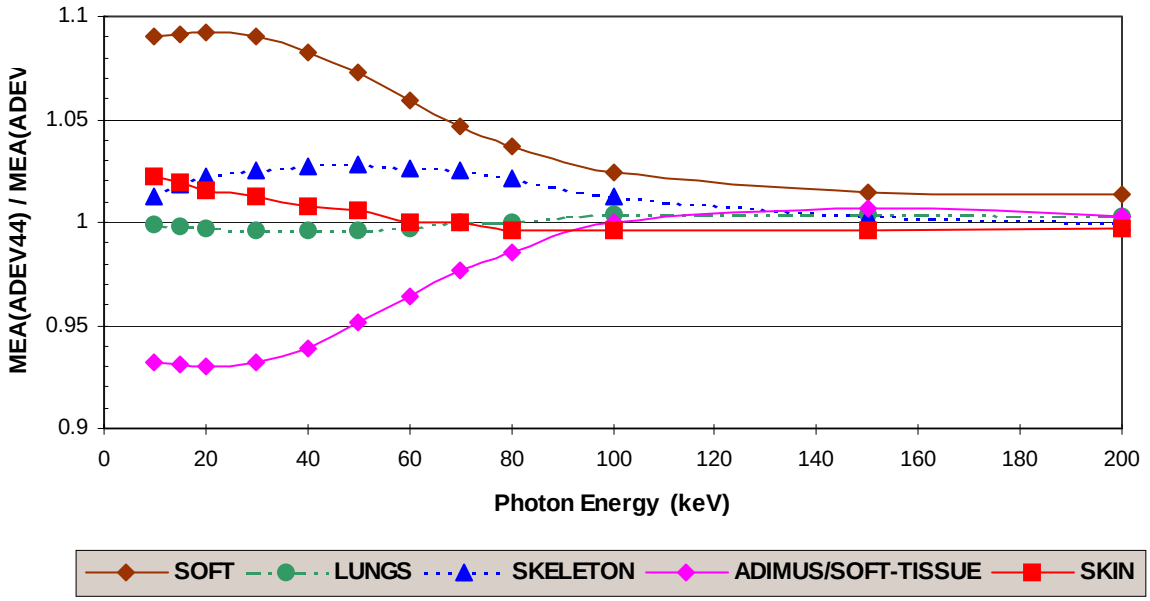

Figure 3. Ratios of mass-energy absorption coefficients

For photon energies up to 200 keV according to the ratios of the mass-energy absorption (MEA) coefficients shown in Figure 3, the replacement of the ADEV by the ADEV44 tissue compositions would lead to an increase of equivalent dose to soft-tissue organs, to the bones, and to the skin. while the lungs equivalent dose would not change significantly. The equivalent dose to the ADIMUS mixture in unspecified regions would be lower than before to the soft-tissue mixture. For the effective dose this is significant, because other tissues surrounded by the ADIMUS mixture experience less shielding than before and consequently their equivalent doses would generally increase.

Anatomies

MHOM/FHOM: The MAX and FAX phantoms connected to the EGS4 Monte Carlo code with ICRU44 tissue compositions, with the same *homogeneous* mixture in all skeletal voxels, and for adipose and muscle in all unspecified regions of the body used for c).

The MAX and the FAXht phantoms have heterogeneous skeletal tissue distributions among the voxel of their skeletons, which was realized by the CT number method described in Kramer et al [11]. For the mathematical phantoms ADAM44 and EVA44 this cannot be achieved, because their construction is not based on digital CT images with grey values, and also separately segmented regions for adipose and muscle are not available for the mathematical phantoms.

In order to compare the dosimetric effects of the different anatomies only, a MAXHOM and a FAXhtHOM phantom were derived from the MAX and the FAXht phantom, respectively, based on the following changes:

all skeletal voxels of the MAXHOM and the FAXhtHOM phantoms have the ADEV44 skeletal mixture from Table I, and all segmented regions of adipose and muscle in the MAXHOM and the FAXhtHOM phantom have the ADIMUS mixture from Table I.

Heterogeneous skeleton and adipose-muscle distribution

MAX/FAX: The MAX and FAXht phantoms connected to the EGS4 Monte Carlo code with ICRU44 tissue compositions, heterogeneous skeleton and separately segmented regions for adipose and muscle.

3. RESULTS

Conversion coefficients between effective dose and ESAK for tube voltages between 60 and 120 kV are shown in Figure 4 for a posterior-anterior chest radiograph and in Figure 5 for an anterior-posterior examination of the abdomen.

Monte Carlo code (a – b)

The curves ADEV-GSF and ADEV represent the calculations for the ADAM and EVA phantoms connected to the GSF and the EGS4 Monte Carlo code, respectively. The average percentage difference found is 1.9% for the chest radiograph, and 0.9% for the examination of the abdomen, which means that they are smaller than the coefficients of variance reported in section 2.2 for the Monte Carlo codes.

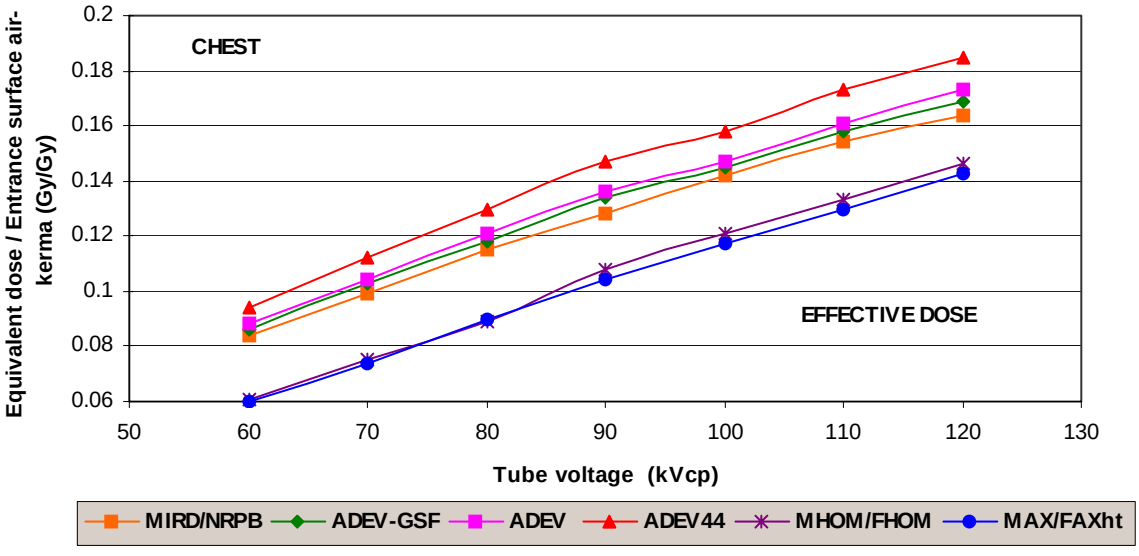

Figure 4. Effective dose conversion coefficients for chest radiograph

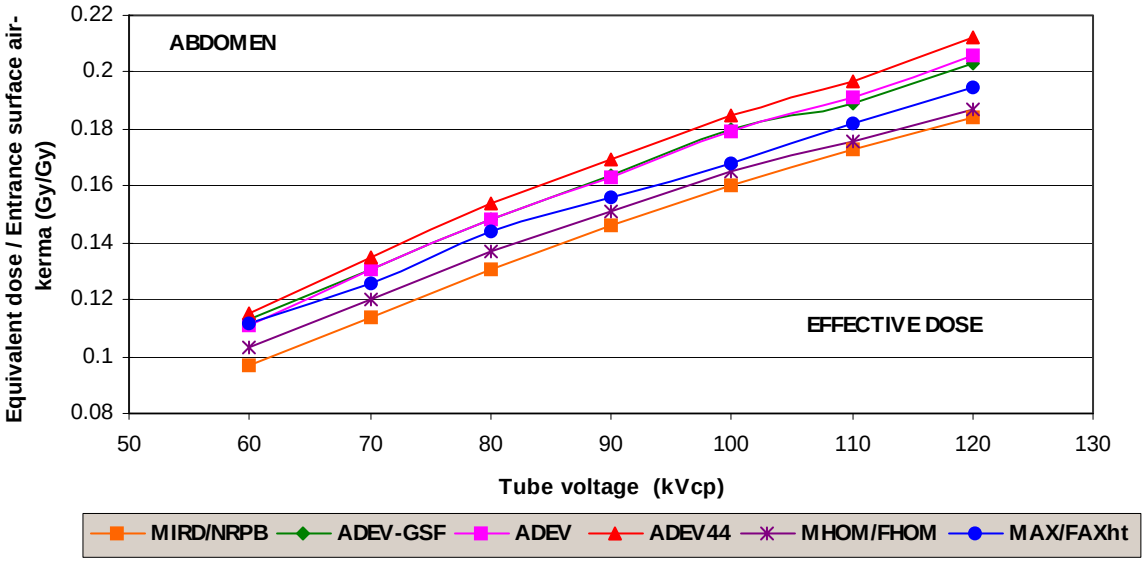

Figure 5. Effective dose conversion coefficients for abdominal radiograph

Tissue composition (b – c)

The curves ADEV and ADEV44 represent the calculations for the ADAM and the EVA phantoms for the two sets of tissue compositions shown in Table I. For both X-ray examinations the ADEV44 curves are significantly greater than the ADEV curves, which confirms the expectations derived from the data shown in Figure 3

Anatomy (c – d)

The effect of replacing the anatomies of the mathematical phantoms by those of the voxel phantoms is demonstrated by the differences between curves ADEV44 and MHOM/FHOM.
Similar to results reported for whole-body exposure to external photon radiation [26, 27], these curves confirm a significant decrease of the effective dose.

The main reasons are:

The anatomic structure of the realistic human skeleton, which causes significantly more shielding to underlying radiosensitive soft-tissue organs compared to the MIRD skeleton. The ribcage of the mathematical phantoms, for example, has no sternum, and the ribs are a set of equidistantly spaced horizontal tori, which allow for a significant unattenuated passage of radiation to reach soft-tissue organs, like the lungs, the thymus, the liver, the stomach, etc. Also, for PA-incidence the naturally shaped and positioned pelvis of the voxel phantoms causes more shielding for the bladder, and the colon than the MIRD pelvis.
The supine position patients usually have during scanning of CT images intensifies this effect,

because soft-tissue organs, like the lungs, the liver, the stomach, etc. could have been shifted more into the ribcage.

The MAX phantom, and especially the FAXht phantom, have generally significantly thicker layers of adipose and muscle compared to the mathematical phantoms, which causes more shielding for underlying radiosensitive organs and tissues.

As for the two radiological examinations considered, this decrease of the effective dose is greater for the chest examination because for PA-incidence the anatomical difference between the two skeletal structures represents the predominant cause for a significant decrease of equivalent dose to radiosensitive organs and tissues contributing to the effective dose, while for the anterior-posterior abdominal radiograph mainly different thicknesses of overlying ADIMUS layers, and differences of organ positions, like for the stomach, and for the colon are the main cause for the decrease.

Heterogeneous skeleton and separately distributed adipose and muscle (d – e)

The dosimetric consequences of the introduction of heterogeneously distributed skeletal tissues and separately distributed adipose and muscle can be seen in Figures 4 and 5 from the difference between the curves MHOM/FHOM and MAX/FAXht.

As for the abdominal AP radiograph, the equivalent doses to the contributing important organs and tissues, like gonads, colon, stomach, bladder, liver, etc. are not significantly affected by overlying skeletal structures, but rather by overlying adipose and/or muscle. Both voxel phantoms, especially the FAXht phantom, have for AP-incidence relatively thick layers of adipose overlying many radiosensitive organs and tissues. While the ADIMUS mixture has a density of 1.012 gcm^{-3} , adipose has a density of 0.95 gcm^{-3} , which means that abdominal organs and tissues lying under layers of adipose would receive higher equivalent doses because of reduced shielding, which leads to an increase of the MAX/FAX effective dose relative to the MHOM/FHOM effective dose.

For the PA chest examination the difference between the MAX/FAXht and the MHOM/FHOM effective dose is mainly a function of the density changes in skeletal structures, like the ribcage, and the spine, and to a lesser extent because of the separately distributed adipose and muscle. Compared to the skeletal density of 1.469 gcm^{-3} for the MHOM/FHOM skeleton, the average skeletal densities in the MAX/FAXht ribcages are 1.52 gcm^{-3} and in the spines 1.27 gcm^{-3} , respectively. For tube voltages up to 85 kV more shielding by the ribcages on the one hand, and less shielding by the spines and the adipose on the other hand cancel each other out, while for energies above 90 kV the net effect is less shielding, i.e. greater equivalent doses to radiosensitive organs and tissues, and therefore an increase of the effective dose.

One can conclude that for given exposure conditions, tissue composition, and position the equivalent dose to an organ or tissue of the human body is basically a function of the compositional and structural shielding caused by the tissues in its vicinity.

Figures 4 and 5 show also the MIRD/NRPB data [3, 6, and 8] calculated for a hermaphrodite MIRD-type phantom with male body dimensions. Compared to the ADEV-GSF effective dose

one expects the MIRD/NRPB effective dose to be somewhat smaller, because for the same organs and tissues the female equivalent doses are generally greater than those for the male body. For the chest radiograph shown in Figure 4 the average difference between the MIRD/NRPB and the ADEV-GSF curve is ca. 3%, which corresponds to this expectation. However for the abdominal examination shown in Figure 5 the MIRD/NRPB effective dose is on average 12.7% smaller than the ADEV-GSF effective dose. For the time being no reasonable explanation has been found for this difference.

4. CONCLUSIONS

In order to investigate the dosimetric consequences for the effective dose if a MIRD-based exposure model is replaced by a voxel-based model, various parameters, like the Monte Carlo code, the compositions of body tissues, and the phantom anatomy, have been considered separately.

The data shown in the previous section demonstrate that the change of the Monte Carlo code had no significant impact on the effective dose, while the update of the tissue compositions with the ICRU44 data led to an increase of the effective dose of 7.4% on average for the chest radiograph, and of 3.4% on average for the abdominal examination.

The replacement of the mathematical phantoms by true to nature human anatomies causes generally a decrease of the effective dose, which is 27.7% on average for the chest radiograph, and 10.9% on average for the abdominal examination.

The introduction of a heterogeneous skeleton, and of separately segmented regions for adipose and muscle can have an increasing or a decreasing effect on the effective dose, depending on the densities of the bones, and the masses of adipose and muscle located inside the X-ray beam volume.

For the complete replacement of the ADEV-GSF exposure model by the MAX/FAXht-EGS4 exposure model a net decrease of the effective dose of 22.4% on the average was found for the chest radiograph, and of 3.8% for the abdominal examination.

ACKNOWLEDGEMENT

The authors would like to thank CNPq and FACEPE for the financial support.

REFERENCES

1. Kramer R. and Drexler G., Zum Verhaeltnis von Oberflächen- und Körperdosis in der Roentgendiagnostik, 7. Wissenschaftliche Tagung der Deutschen Gesellschaft fuer Medizinische Physik e.V., Heidelberg, 5.-7.5.1976, In: *Medizinische Physik*, **Band 2**, p. 683-695, Herausgegeben von W.J.Lorenz, Huethig Verlag, Heidelberg, (1976).

2. Rosenstein M., *Organ doses in Diagnostic Radiology*, US Department of Health, Education and Welfare, Bureau of Radiological Health, BRH Tech., Publ. DA 76-8030, (1976).
3. Jones D. G. and Wall B. F., *Organ Doses from Medical X-ray Examinations Calculated Using Monte Carlo Techniques*, National Radiological Protection Board, Chilton, Didcot, Oxon OX11 0RQ, UK, NRPB-R186, (1985).
4. Drexler G., Panzer W., Widenmann L., Williams G. and Zankl M., *The Calculation of Dose from External Photon Exposures Using Reference Human Phantoms and Monte Carlo Methods, Part III: Organ Doses in X-Ray Diagnosis*, Institut für Strahlenschutz, GSF-Gesellschaft für Umwelt und Gesundheit, D-8042 Neuherberg, GSF-Bericht 11/90, (1990).
5. Le Heron J. C., Estimation of effective dose to the patient during medical x-ray examinations from measurements of the dose-area product, *Phys. Med. Biol.*, **Vol. 37**, No.11, 2117-2126, (1992).
6. Hart D., Jones D. G. and Wall B. F., *Estimation of Effective Dose in Diagnostic Radiology from Entrance Surface Dose and Dose-Area Product Measurements*, National Radiological Protection Board, Chilton, Didcot, Oxon OX11 0RQ, UK, NRPB-R262, (1994).
7. Servomaa A. and Tapiovaara M., Organ Dose Calculation in Medical X-Ray Examinations by the Program PCXMC, *Rad. Prot. Dos.*, **Vol. 80**, Nos 1-3, pp.213-219, (1998).
8. Hart D., Jones D. G. and Wall B. F., *Normalised Organ Doses for Medical X-ray Examinations Calculated using Monte Carlo Techniques*, National Radiological Protection Board, Chilton, Didcot, Oxon OX11 0RQ, UK, NRPB-SR262, (1994).
9. Zankl M., Panzer W. and Herrmann C., Calculation of Patient Doses Using a Human Voxel Phantom of Variable Diameter, *Rad. Prot. Dos.*, **Vol. 90**, Nos 1-2, pp.155-158, (2000).
10. Akahane K., Kai M., Kusama T. and Saito K., *Dose estimation of patients from diagnostic X-ray based on CT-voxel phantom*, Proceedings of the Ninth EGS4 Users' Meeting in Japan, KEK Proceedings 2001-22, p.87-91, (2001).
11. Kramer R., Vieira J. W., Khoury H. J., Lima F. R. A. and Fuelle D., All About Max: A Male Adult Voxel Phantom for Monte Carlo Calculations in Radiation Protection Dosimetry, *Phys. Med. Biol.*, **48**, No.10, 1239-1262, (2003).
12. Loureiro E. C. M., Kramer R., Vieira J. W., Khoury H., Lima, F. R. A. and Hoff G., Construction of the FAXht (Female Adult voXel) head+trunk phantom from CT images of patients for applications in radiation protection, submitted to IRPA11, (2004).
13. Nelson W. R., Hirayama H. and Rogers D. W. O. *The EGS4 Code System* SLAC-265 Stanford Linear Accelerator Center, Stanford University, Stanford, California, (1985).
14. ICRP - 1990 Recommendations of the International Commission on Radiological Protection. *ICRP Publication 60* International Commission on Radiological Protection, Pergamon Press, Oxford, (1991).
15. Kramer R., Zankl M., Williams G., Drexler G., The Calculation of Dose from External Photon Exposures Using Reference Human Phantoms and Monte Carlo Methods. Part I: The Male (ADAM) and Female (EVA) Adult Mathematical Phantoms. GSF-Report S-885.Reprint July 1999.Institut für Strahlenschutz, GSF-Forschungszentrum für Umwelt und Gesundheit, Neuherberg-München, (1982).
16. Snyder W. S., Ford M. R., Warner G. G., Watson G. G., Revision of MIRD Pamphlet No. 5 Entitled "Estimates of absorbed fractions for monoenergetic photon sources uniformly distributed in various organs of a heterogeneous phantom". ORNL-4979, Oak Ridge National Laboratory, Oak Ridge, Tenn., (1974).
17. ICRP - Report of the Task Group on Reference Man. *ICRP Publication 23*. International Commission on Radiological Protection, Pergamon Press, Oxford, (1975)

18. Kramer R., *Ermittlung von Konversionsfaktoren zwischen Körperdosen und Relevanten Strahlungskenngrößen bei Externer Röntgen- und Gamma-Bestrahlung* Gesellschaft für Strahlen- und Umweltforschung, München-Neuherberg, GSF-Bericht-S-556, (1979).
19. Zankl M., Drexler G., Petoussi-Henss N. and Saito K., *The Calculation of Dose from External Photon Exposures Using Reference Human Phantoms and Monte Carlo Methods. Part VII: Organ Doses due to Parallel and Environmental Exposure Geometries* GSF-Report 8/97. Institut für Strahlenschutz, GSF-Forschungszentrum für Umwelt und Gesundheit, München-Neuherberg, (1997).
20. Warner G. G. and Craig A. M., ALGAM: *A Computer Program for Estimating Internal Dose for Gamma-Ray Sources in a Man Phantom*, Oak Ridge National Laboratory, Oak Ridge, Tenn., USA, Report ORNL-TM-2250, (1968).
21. Roussin R. W., Knight J. R., Hubbell J. H. and Howerton R. J., *Description of the DLC-99/HUGO package of photon interaction data in ENDF/B-V format*, Report No. ORNL-RSIC-46 (ENDF-335), Radiation Shielding Information Center, Oak Ridge National Laboratory, Oak Ridge, TN, USA, (1983).
22. ICRP - *ICRP Publication 89*, Basic Anatomical and Physiological Data for Use in Radiological Protection: Reference Values, International Commission on Radiological Protection, Pergamon Press, Oxford, (2003).
23. Storm E. and Israel H. I., Photon Cross-sections from 1 keV to 100 MeV for Elements Z=1 to Z=100, *Atomic Data and Nucl. Tables* **7**, 565, (1970).
24. Hubbell J. H. and Overbo I., Relativistic Atomic Form Factors and Photon Coherent Scattering Cross Sections, *J. Phys. Chem. Ref. Data*, **9**, 69, (1979).
25. Cristy M. and Eckerman K. F., *Specific Absorbed Fractions of Energy at Various Ages from Internal Photon Sources*, ORNL/TM-8381 Vol. 1-7,Oak Ridge National Laboratory, Oak Ridge, Tenn., USA, (1987).
26. Kramer R., Vieira J. W., Khoury H. J., and Lima F. R. A., MAX meets ADAM: A dosimetric comparison between a voxel-based and a mathematical model for external exposure to photons, *Phys. Med. Biol.* (accepted for publication), (2004).
27. Kramer R., Vieira J. W., Khoury H. J., Loureiro E. C. M., Lima F. R. A. and Hoff G., (2004b), *Comparison of effective dose between tomographic and mathematical phantoms for external exposures to photons*, submitted to the 11 Congress of the International Radiation Protection Association, (2004).
28. Cranley K., Gilmore B. J., Fogarty G. W. A. and Desponds L., *Catalogue of Diagnostic X-ray Spectra and Other Data*, The Institute of Physics and Engineering in Medicine (IPEM), Report No 78, Electronic Version prepared by D Sutton, September (1997).
29. ICRU - Tissue substitutes in radiation dosimetry and measurement, *ICRU Report 44*, International Commission on Radiation Units and Measurements, Bethesda, MD, (1989).
30. ICRP - Basic Anatomical and Physiological Data for use in Radiological Protection: The Skeleton, *ICRP Publication 70*. International Commission on Radiological Protection, Pergamon Press, Oxford, (1995).